SCIENCE CHINA
Technological Sciences

• Article •

April 2014 Vol.57 No.4: 819–827
doi: 10.1007/s11431-014-5506-4

Validation of dynamic cavitation model for unsteady cavitating flow on NACA66

ZHANG XiaoBin, ZHANG Wei, CHEN JianYe, QIU LiMin & SUN DaMing*

Institute of Refrigeration and Cryogenics, Zhejiang University, Hangzhou 310027, China

Received December 5, 2013; accepted January 26, 2014

Unsteady cavitating flow is extremely complicated and brings more serious damages and unignorable problems compared with steady cavitating flow. CFD has become a practical way to model cavitation; however, the popularly used full cavitation model cannot reflect the pressure-change that the bubble experiences during its life path in the highly unsteady flow like cloud cavitating. Thus a dynamic cavitation model (DCM) is proposed and it has been considered to have not only the first-order pressure effects but also zero-order effect and can provide greater insight into the physical process of bubble producing, developing and collapsing compared to the traditional cavitation model. DCM has already been validated for steady cavitating flow, and the results were reported. Furthermore, DCM is designed and supposed to be more accurate and efficient in modeling unsteady cavitating flow, which is also the purpose of this paper. The basic characteristic of the unsteady cavitating flow, such as the vapor volume fraction distribution and the evolution of pressure amplitude and frequency at different locations of the hydrofoil, are carefully studied to validate DCM. It is found that not only these characteristics mentioned above accord well with the experimental results, but also some detailed transient flow information is depicted, including the re-entrant jet flow that caused the shedding of the cavity, and the phenomenon of two-peak pressure fluctuation in the vicinity of the cavity closure in a cycle. The numerical results validate the capability of DCM for the application of modeling the complicated unsteady cavitating flow.

unsteady cavitation, dynamical cavitation model, NACA66, hydrofoil

Citation: Zhang X B, Zhang W, Chen J Y, et al. Validation of dynamic cavitation model for unsteady cavitating flow on NACA66. Sci China Tech Sci, 2014, 57: 819–827, doi: 10.1007/s11431-014-5506-4

1 Introduction

Cavitation is defined as the formation of vapor bubbles in a flow when the local pressure falls below the liquid's saturation vapor pressure. Cavitation in hydraulic machines causes unignorable problems, such as vibration, lift fluctuation and erosion of solid surface. Most of these problems, especially the erosion, are related to the transient behavior of cavitation phenomenon.

In the last decades, different mathematical formulations for modeling cavitation were developed based on the mixture model, which treats the two-phase flow as a single vapor-liquid phase mixture flow, and the momentum exchange between two phases is usually ignored. For instance, the approach of mixture equation of state (EOS) calculating the vapor fraction requires an additional EOS [1–3]. While, it fails to model the complex re-entrant vortex flow in the wake of the cavity since the vortex term $\nabla P \times 1/\rho$ equals zero [4]. Recently, the transport equation-based strategy [5–7] has become the most popular numerical method to simulate the cavitation. The vaporization/liquefaction rate is considered as the source of the supplemented transport equation of vapor volume/mass fraction, which makes the simulation of surface tracking and reflection of the vortex characteristic of the wake of the cavity possible. The calculation of the va-

*Corresponding author (email: sundaming@zju.edu.cn)

porization/liquefaction rate, also called the cavitation model, is the key to ensure the accuracy of the numerical method. The popular cavitation model includes the Merkle model [8], Kunz model [9], interfacial dynamic-based model [10] and the full cavitation model [5]. Other model, such as Sauer model [11], was also reported. Among them, the full cavitation model (FCM) developed by Singhal considers all the pressure first-order effects and has been well proven in modeling of the quasi-steady cavitation flow for thermosensible [12,13] and non-thermosensible fluids [14]. Recently, the application of FCM to the modeling of 3D unsteady cavitating flow of the twist hydrofoil was also reported [15,16]. In their calculations, the standard k-ε turbulence closure and the wall function were used, and the model coefficients had to be modified to obtain the qualitatively exact results compared to the experimental observations. The bubble radius in FCM is assumed to be the maximum possible value during the cavitation process, which is suitable for the quasi-steady cavitation, such as the attached sheet cavitation. However, the pressure-change that the bubble experiences during its life path in the highly unsteady flow like cloud cavitating, is so large that the assumption above is not available and the bubble radius cannot be treated as a constant. Therefore, there is still room for improvement in the accuracy of modeling unsteady cavitation with FCM.

A dynamic cavitation model (DCM) was developed to improve FCM, which ignores the pressure zero-order effects in calculating the bubble radius [17]. In DCM, the Rayleigh-Plesset equation is used to calculate the pressures difference in bubble interface. And the Gibbs-Duhem equation is used to obtain the dynamic relationships of the pressure across the bubble by assuming the thermodynamic equilibrium during the cavitation process. This assumption is proved to be valid based on the fact: Examinations of temperature and pressure data for cavitation in Freon and the thermosensible fluid of liquid nitrogen [18] reveal that the saturation vapor pressure matches the local pressure measurement. Combining these two equations, one obtains the pressure dependent bubble radius. Then it is substituted into the FCM model for recalculation of the bubble radius and leads to DCM. As the bubble radius is local pressure dependent, DCM is supposed to have the potential to provide deeper insight into the physics of the unsteady cavitating flow than FCM.

The performance of DCM applying to the modeling of the quasi-steady sheet cavitating flow has been well validated in our previous paper [17]. Now, this paper aims to further evaluate the potentials and performance of modeling the unsteady cloud cavitating flow. The computations are based on the homogenous mixture model with an additional transport equation of gas mass fraction. The converged solutions are obtained with the CFD software package Fluent 6.3, and DCM is implemented as a source term into the mass fraction transport equation. The validations of DCM are performed by modeling the steady and unsteady cavitating flows through the NACA66 hydrofoil. By comparing with the experimental results, the numerical results validate the capacity of DCM in modeling and capturing the complex physics of the unsteady cavitating flow.

2 CFD model

For water, the cavitation process is considered to be isothermal, so the energy conservation equation is not solved. The set of governing equations for cavitation based on the homogenous equilibrium flow model comprises the conservative form of the Navier-Stokes equation, the k-ε two-equation turbulence closure and a transport equation for the vapor mass fraction, the continuity and momentum equations for the unsteady flow are given below, respectively [5]:

$$\frac{\partial}{\partial t}(\rho_{\mathrm{m}})+\frac{\partial}{\partial x_j}(\rho_{\mathrm{m}}u_j)=0\,, \tag{1}$$

$$\frac{\partial}{\partial t}(\rho_{\mathrm{m}}u_i)+\frac{\partial}{\partial x_j}(\rho_{\mathrm{m}}u_iu_j)=-\frac{\partial P}{\partial x_i}+\frac{\partial \tau_{ij}}{\partial x_j}\,, \tag{2}$$

$$\tau_{ij}=(\mu+\mu_t)\left(\frac{\partial u_i}{\partial x_j}+\frac{\partial u_j}{\partial x_i}\right)\delta_{ij},\delta_{ij}=1,\ i=j;\ \delta_{ij}=0,\ i\neq j, \tag{3}$$

where x and the indices i, j and k denote the coordinate axes, t is time, u is the velocity vector, P is pressure, μ is viscosity, and ρ_{m} is the mixture density, defined as

$$\rho_{\mathrm{m}}=\alpha_{\mathrm{g}}\rho_{\mathrm{g}}+\alpha_{\mathrm{v}}\rho_{\mathrm{v}}+(1-\alpha_{\mathrm{g}}-\alpha_{\mathrm{v}})\rho_{\mathrm{l}}, \tag{4}$$

where m is for mixture, α represents the volume fraction, and the subscripts v, g, and l denote, respectively, the vapor phase, non-condensable gas, and liquid phase. The effect of slip velocity between the liquid and vapor phases on the momentum exchange has been neglected in eq. (2) because cavitation often occurs in region of high-speed flow. The realizable k-ε turbulence model, which shows substantial improvements in computing flows with sharp streamline curvature or vortices compared with the standard k-ε model, has been adopted [19,20].

The vapor mass fraction f in a cavitation process is determined by solving the transport equation as follows:

$$\frac{\partial}{\partial t}(f\rho_{\mathrm{m}})+\nabla\cdot(f\rho_{\mathrm{m}}u_{\mathrm{v}})=\dot{R}, \tag{5}$$

where $\dot{R}$ is the net evaporation or condensation rate depending on the system, u_v is the velocity of vapor phase. Singhal et al, have utilized the Rayleigh-Plesset equation for bubble dynamics to deduce an expression for $\dot{R}$ as

$$\dot{R}=\frac{3\alpha_{\mathrm{v}}\rho_{\mathrm{v}}\rho_{\mathrm{l}}}{R_{\mathrm{b}}}\sqrt{\frac{2(P_{\mathrm{b}}-P)}{3\rho_{\mathrm{l}}}}, \tag{6}$$

where R_b is the single bubble radius and is determined by using the maximum possible value $R_b = 0.061We\sigma / (0.5\rho u_{rel}^2)$ [5]. Thus, it is independent of the local pressure, and potentially an improper way to consider the dynamic nature of the cavitation process that the bubble experiences large pressure variance, especially for cloud and vortex cavitation. Based on thermodynamic equilibrium between the two phases, the present authors used the Gibbs-Duhem equation and the Rayleigh-Plesset equation to calculate the pressure-dependent R_b, and then obtained the following dynamic cavitation model (DCM) in our previous studies. More details are described in ref. [17].

For evaporation process (when $P_{sat} > P$)

$$\dot{R}_e = C_e\rho_v(1-f_g-f_v)\frac{P_{sat}(T)\exp\{[P-P_{sat}(T)]/(\rho_l RT)\}-P}{\sigma}\sqrt{\frac{2(P_{sat}-P)}{3\rho_l}}, \quad (7)$$

for condensation process (when $P_{sat} \leqslant P$)

$$\dot{R}_c = C_c\rho_l f_v \frac{\rho_l RT\ln[P/P_{sat}(T)]+P_{sat}(T)-P}{\sigma}\sqrt{\frac{2(P-P_{sat})}{3\rho_l}}, \quad (8)$$

where C_e, C_c are empirical constants, here C_e=0.02, C_c=0.01; f_g is the mass fraction of non-condensable gas, σ is surface tension. In isothermal cavitation like water, saturated pressure and surface tension are both constants, thus bubble radius depends on local pressure only.

For comparison, the original full cavitation model [5] is shown below:

$$\dot{R}_e = C_e\rho_v\rho_l(1-f_g-f_v)\frac{\sqrt{k}}{\sigma}\sqrt{\frac{2(P_{sat}-P)}{3\rho_l}}, \quad P_{sat} > P, \quad (9)$$

$$\dot{R}_e = C_c\rho_l\rho_l f_v \frac{\sqrt{k}}{\sigma}\sqrt{\frac{2(P-P_{sat})}{3\rho_l}}, \quad P_{sat} \leqslant P. \quad (10)$$

3 Methodology

Figure 1 shows the geometry of NACA66 and the grid scheme in the forthcoming simulations. The relative maximum thickness of the hydrofoil is τ=12% at 45% from the leading edge, and the relative maximum camber ratio is 2% at 50% from the leading edge with the chord length c=0.15 m. Comparisons of the calculations are performed mainly with the experimental observations [21], in which one set of pressure monitors is aligned along the chord on the suction side from x/c=0.05 up to the trailing x/c=0.90 with a step of 0.10c from x/c =0.10.

The k-ε turbulence model has been widely used to model the cavitating flows, which can catch the general features of

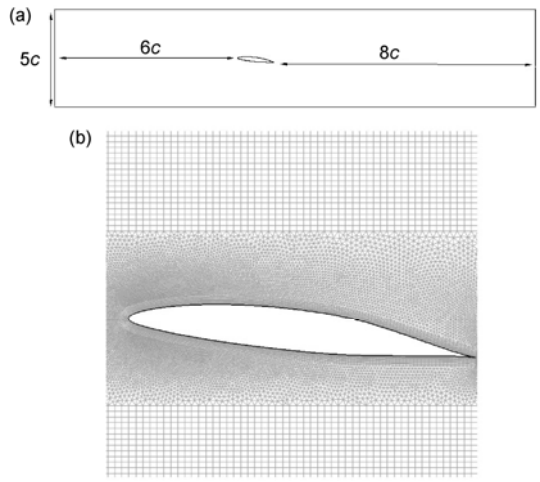

Figure 1 Geometry and computational grid of NACA66. (a) Geometry; (b) close up view of grid scheme.

turbulent cavitating flow [19,20]. While, some researchers pointed out that the original k-ε model tended to overpredict the turbulent eddy viscosity in the rear part of the cavity. Therefore, the LES [22] and the turbulent viscosity modified k-ε model [18,23] have been suggested for more rigorous modeling of the complex cavitating flow. The boundary conditions of the simulations are velocity inlet and pressure outlet. The convective term is discretized using the second-order accurate upwind scheme and the other terms like vapor mass fraction, two turbulent equations, are first-order upwind scheme. The density and dynamic viscosities of liquid water are taken to be ρ_l=998.12 kg/m^3 and μ_l= 9.9710^{-4} Pa s at temperature of 293 K. The vapor density of water is ρ_v=0.0175 kg/m^3 and the vapor viscosity is μ_v=9.732510^{-6} Pa s, and the saturated pressure at 293 K is P_v=2367 Pa. The mass fraction of the non-condensable gas in the bubble is set to be 10^{-8} to avoid its effects. The cavitation number σ is defined as

$$\sigma = \frac{P_i - P_v}{0.5\rho u_i^2}, \quad (11)$$

where P_i is the inlet pressure, u_i is the inlet velocity. Another important dimensionless number used to describe the flow field is the discharge coefficient C_p:

$$C_p = \frac{P - P_i}{0.5\rho u_i^2}, \quad (12)$$

where P is the local pressure. It is found that the time step size (Δt) has a great effect on the simulations of unsteady cavitation [2,21]. A temporal convergence study is carried out in the case of partial sheet cavitation by DCM with σ=1.25. The pressure fluctuation at x/c=0.5 under different time step sizes is depicted in Figure 2. The period of the pressure fluctuation depends on Δt greatly that the pressure cycle decreases when Δt decreases from 5×10^{-4} to 110^{-4} s,

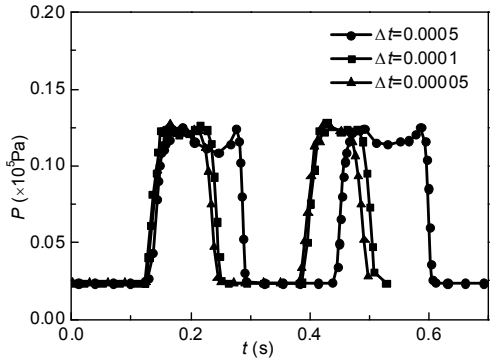

Figure 2 Calculated pressure fluctuation at x/c=0.5 with DCM at different time step sizes at σ=1.25.

while, it does not vary much when Δt further decreases to 510^{-5} s. In addition, Figure 3 shows the computational time-averaged C_p along the suction surface of the hydrofoil. It is found that these values of different Δt yield very similar results, hence Δt=110^{-4} s is chosen for the computations. The non-dimensional value of y+ along the suction side of the hydrofoil is about 10.2. In our previous studies [12], the value of y+<100 in cavity core zone can ensure the grid-independent solutions for k-ε turbulence closure.

4 Results and analyses

4.1 Steady flow (σ=1.34)

The length of the cavity remains stable when σ=1.34, as shown in Figure 4. The ratio of cavity length to chord length is l/c=0.37 using DCM, while the experiment's is 0.4. Figure 5 shows the pressure fluctuation intensity of the same position of the experimental pressure monitors along the suction side, which is defined as the ratio of RMS of the pressure fluctuations $P_{\text{rms}} = \sqrt{\sum (P-\bar{P})^2 / n}$ to the dynamic pressure $q = 0.5\rho u_i^2$, where $\bar{P}$ is the time-averaged pressure. It is found that in the majority of cavity zones the fluctuation intensity is less than 5%, except in the vicinity

Figure 4 Contour of the density with DCM at u=5.33 m/s and σ=1.34.

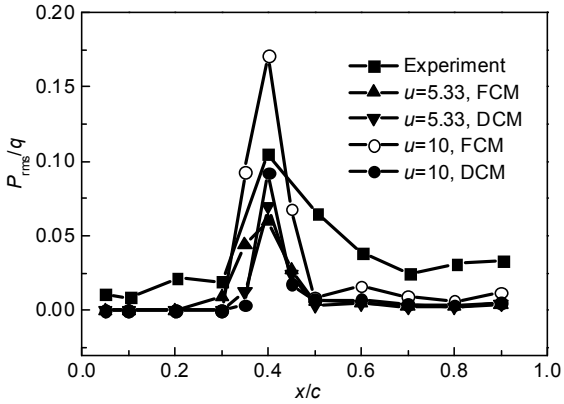

Figure 5 Pressure fluctuation intensity at different monitors (σ=1.34).

of the rear (x/c~0.4), where the calculated maximum by DCM is 10%, approximately the same as the experimental measurement. As a whole, the fluctuation intensity is so small that it can be neglected, thus it is reasonable and acceptable that the flow is considered as a quasi-steady flow when σ=1.34. The fluctuation intensity of DCM is found to be a little smaller than the experiment's on the whole, while, almost the same as FCM except at the rear of the cavity, where the results of FCM are much larger than the experiment's.

Figure 6 shows the comparisons of the calculated distributions of time-averaged C_p along the suction side of the NACA66 hydrofoil using DCM and FCM with the experimental data. The calculated curves by the two cavitation models almost coincide, and the length of constant C_p region is about 0.36c. Considering that the length stands for

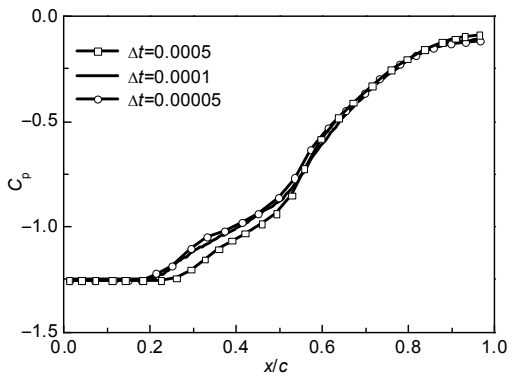

Figure 3 Time-averaged pressure coefficients with DCM at different time step sizes at σ=1.25.

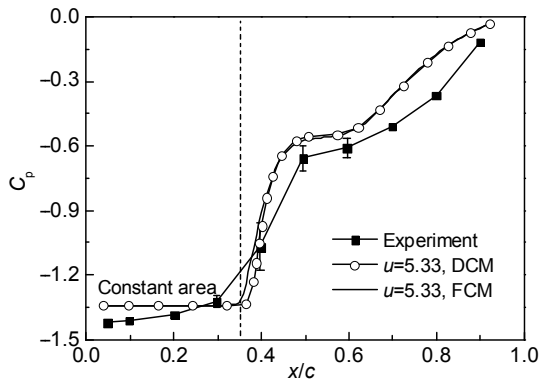

Figure 6 Pressure coefficient distribution along hydrofoil at u=5.33 m/s at σ=1.34.

the length of the cavity core, we can safely say DCM performs equivalent to FCM in computing the steady cavity. In the cavity core, the computed C_p value is about −1.34, which is a little higher than the experiment and equals the minus cavitation number (C_p–σ), which means the local pressure approaches to the saturated one (P–P_v) according to eqs. (9) and (10). In the wake of the cavity, the C_p changes abruptly, and the increasing slope is larger than the experiment results, which indicates that the computed two-phase zone is smaller. In the trail edge of the hydrofoil, the C_p of DCM is also almost the same as FCM, while, both are much higher than the experiments.

The effects of *Re* on the cavitation flow are investigated. Three inlet velocities are used to get different Reynolds numbers, that is u=5.33, 10, 15 m/s, corresponding to the *Re* of 0.810^6, 1.510^6, 2.2510^6, respectively. Figure 7 describes the distributions of the water volume fraction α_l along the hydrofoil with different *Re*. It is easy to find that the length of the cavity decreases with the increase of *Re*, which primarily attributes to the changes of the pressure fluctuation intensity shown in Figure 5. The P_{rms}/q at x/c=0.4 increases when the inlet velocity increases from 5.33 to 10 m/s, which means the wake of the cavity becomes more turbulent and is easier to break off, thus harder to maintain the cavity length. In addition, the volume fraction curves become steeper, implying that the boundary between two phases becomes more evident and the mixture area becomes smaller in the wake of the cavity.

4.2 Unsteady flow (σ=1.25)

The P_{rms}/q becomes increasingly larger when σ drops to 1.25 from 1.34, as shown in Figure 8. Compared to Figure 5 for σ=1.34, the pressure fluctuations appears not only at the rear of the cavity zone, but also in the whole cavity zone. The maximum of P_{rms}/q is about 0.31. The difference between the experiments and DCM becomes larger. In the cavity core, the computational results of DCM are relatively small and more close to the experimental values compared to FCM, of which the results are much larger than the experiments. In the recovering zone, both results are smaller than the experiments, and the results of FCM are more close to the experiments. While, in view of the fluctuating characteristics of the local pressure, these results agree well, especially at the middle of the hydrofoil.

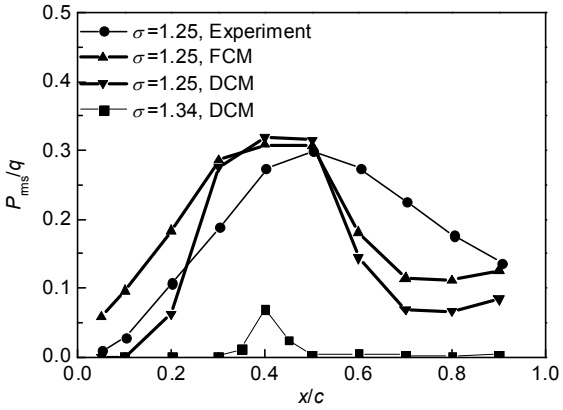

Figure 8 Pressure fluctuation intensity at different cavitation numbers with DCM and FCM.

The transient C_p in a semi-cycle is depicted in Figure 9, which reflects the developing and collapsing of the cavity. The cavity becomes larger and larger since t=0.686 s and reaches the largest when t=0.854 s. After that the second half cycle begins, the length of constant C_p decrease. Though the transient C_p (0.686 s<t<0.770 s) of DCM and FCM in the cavity zone is higher than the experiment in Figure 9, the time-averaged C_p of DCM and FCM agree very well with the experiment, as shown in Figure 10. In the range of x/c=0.0–0.2, the length of constant C_p of DCM is close to the experiment while that of FCM is a little smaller. At the middle of hydrofoil (x/c=0.3–0.6), the results of DCM are more close to the experiment. The results are almost the same in the left range of the hydrofoil where the bubbles detach from the wall and the re-entrant jet flow makes the pressure and the calculated C_p at the wall increase so sharply that both calculations depart from the experiments more obviously. The comparisons of the transient

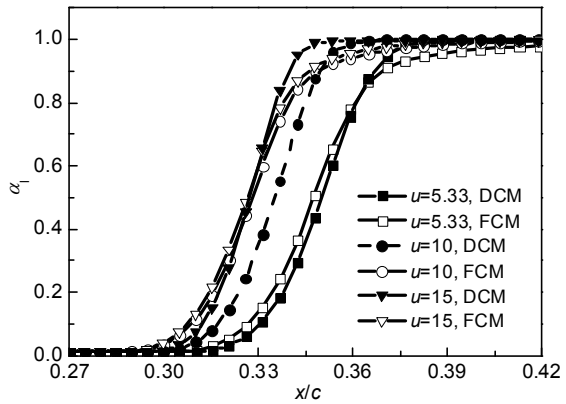

Figure 7 Water volume fraction distribution along the hydrofoil at σ=1.34.

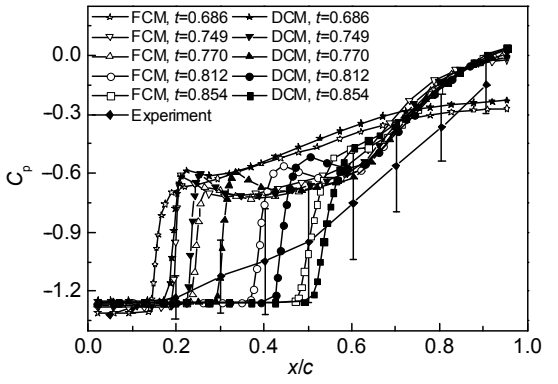

Figure 9 Transient C_p distributions in a semi cycle. Vertical bars are P_{rms}/q.

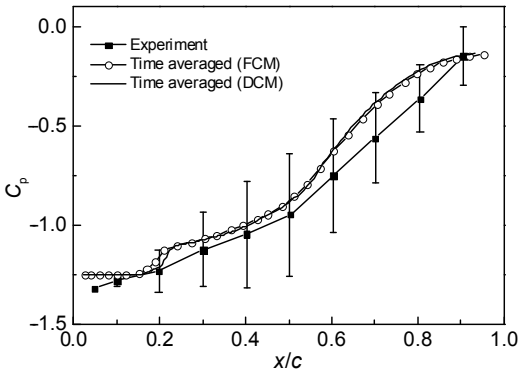

Figure 10 Time-averaged C_p of DCM and FCM at σ=1.25.

volume fraction α of DCM and FCM are shown in Figure 11. The length of the cavity of DCM seems to grow faster, implying that the cycle time of DCM is smaller and the cavity grows faster compared to FCM. More will be discussed in Figure 14(b).

Figure 12 gives the contours of the volume fraction α at different times, which shows the transient evolutions of the cavity's developing, shedding and collapsing. The corresponding experimental observations [21] at the same process are also given for comparisons. Qualitatively, they are well accordant. A long and narrow cavity is formed in the leading edge at t=1.26 s, then it grows larger along the wall of the hydrofoil. When the length is more than about 0.5c, the trailing of the cavity becomes so unstable that the cavity breaks off and sheds from the wall. At the same time, the length of the cavity that adheres to the wall becomes smaller in Figures 12 (f)–(g).

The streamlines and vortex in the wake of the cavity at different times are depicted in Figure 13. The vortex is not formed at x/c=0.1 when t=1.26 s. As time elapses, the cavity develops and the vortex becomes intensive, which makes the wake of the cavity unsteady and induces the re-entrant jet flow to appear in the wake as shown in Figure 13(b). When the vortex becomes intensive enough, the wake of the cavity starts to shed off the wall and the length that adheres

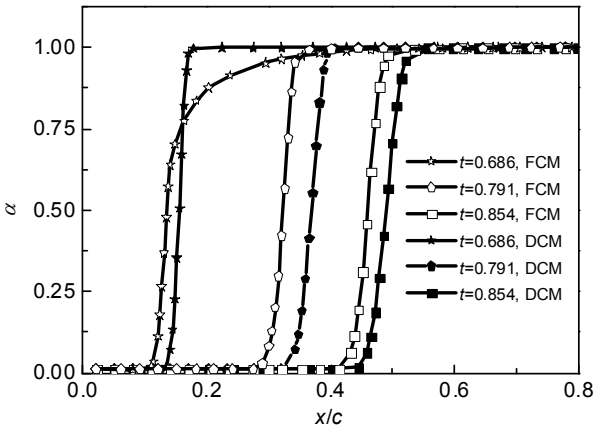

Figure 11 Transient α_l distributions of DCM and FCM at different times.

to the wall becomes smaller under the effects of the re-entrant jet flow (Figure 13(c)), as described by the other authors [24–26].

Periodical pressures at x/c=0.3, 0.5 and 0.7 during cavity growth/destabilization cycle from the calculations and measurements [21] are shown in Figure 14. Taking the pressure at x/c=0.5 for an example, the period of DCM is 0.292 s while the values of experiment and FCM are 0.276 and 0.297 s, respectively. The calculated frequencies are both lower than the experimental data and the relative error of DCM is 5.80%, surprisingly close to the experiment, as shown in Table 1. The picture inside the circle in Figure 14(b) also shows that the cycle time of DCM is smaller and is more close to the experiment than FCM. The results are accordant with the results in Figure 11 where the C_p of FCM seems to have a phase delay compared to DCM. The computed magnitudes of pressure in Figure 14(b) agree well with the experimental values except a few points, which validates the ability of DCM of predicting the pressure fluctuation.

In Figure 14, the magnitude of maximum pressure of DCM and FCM is relatively small compared to the experiments at x/c=0.3. The shape of unsteady pressure curves of DCM coincides more with the experiments while the duration of wave crest of FCM is larger than the experiments. Though the period of both models agree well with the experiment at x/c=0.7, much difference exists in the magnitude of pressure amplitude between the calculations and experiments, which is also reflected in Figure 8. The possible reason is that the unsteady and stochastic impact of single bubble on the wall leads to the irregular fluctuations of pressures in the experiments. While, in the CFD modeling, the averaged actions of the bubble group rather than a single bubble are simulated, so the results of CFD seems more regular compared to the experiments. And another possible reason is due to the stream-wise vortex effects as it is clearly indicated by the experimental observations shown in Figure 12 [27,28].

Figure 15 gives the calculated unsteady pressure fluctuations at different positions with DCM. The periodical fluctuation of pressure is the results of the periodical cycle of developing, shedding and collapsing of the cavity. Most of the time, the pressure remains the vaporization pressure of P_v=2367 Pa at x/c=0.3 for σ=1.25. The pressure increases suddenly to the peak when the length of cavity is smaller than 0.3c due to the effects of re-entry jet, and drops down to the vaporization pressure after the cavity length grows to be larger than 0.3c again.

The lowest pressure at x/c=0.5 also keeps the vaporization pressure, which indicates that the maximum length of cavity is more than 0.5c in a cycle. Comparably, the pressure fluctuation starts to decrease and two peaks are formed in a cycle, which is more obvious in the curve for x/c=0.7. The minimum pressure at x/c=0.7 is much higher than the vaporization pressure, as a result of the cavity's collapsing

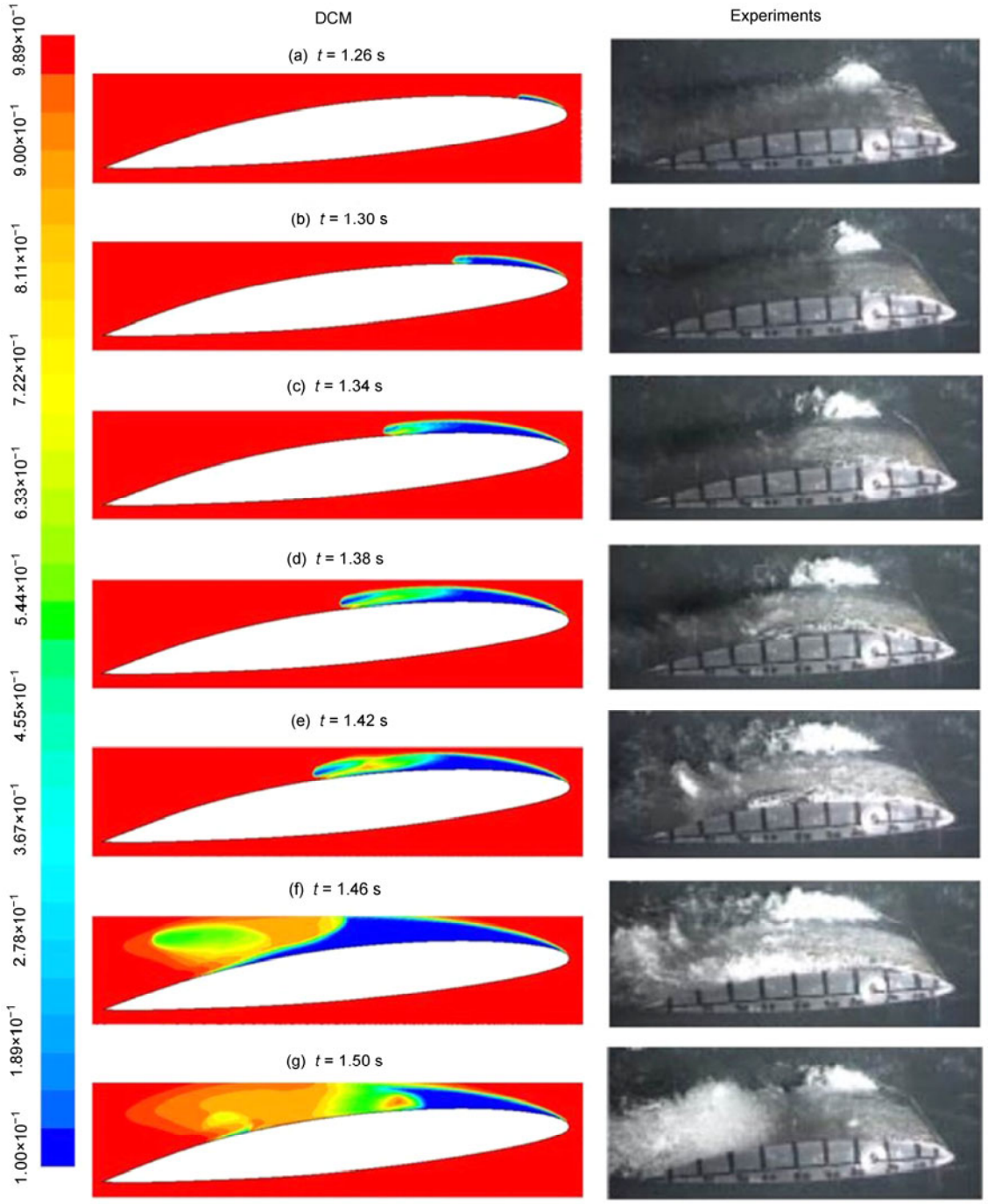

Figure 12 Contours of the water volume fraction of DCM at different times (Fluids flow from right to left).

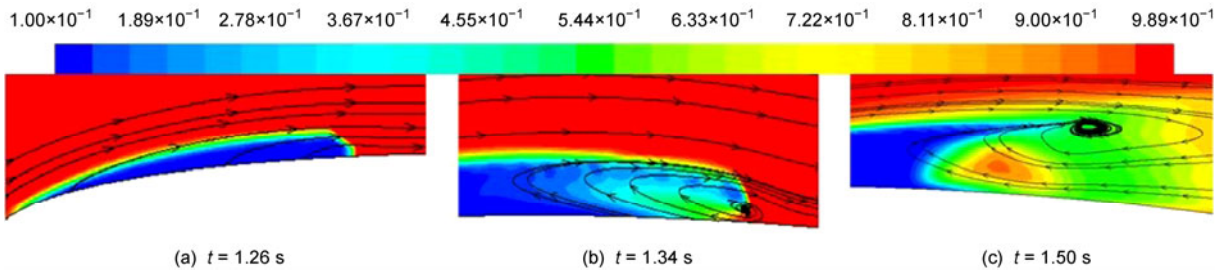

Figure 13 Close-ups of vortex and re-entrant jet flow around the hydrofoil at different times.

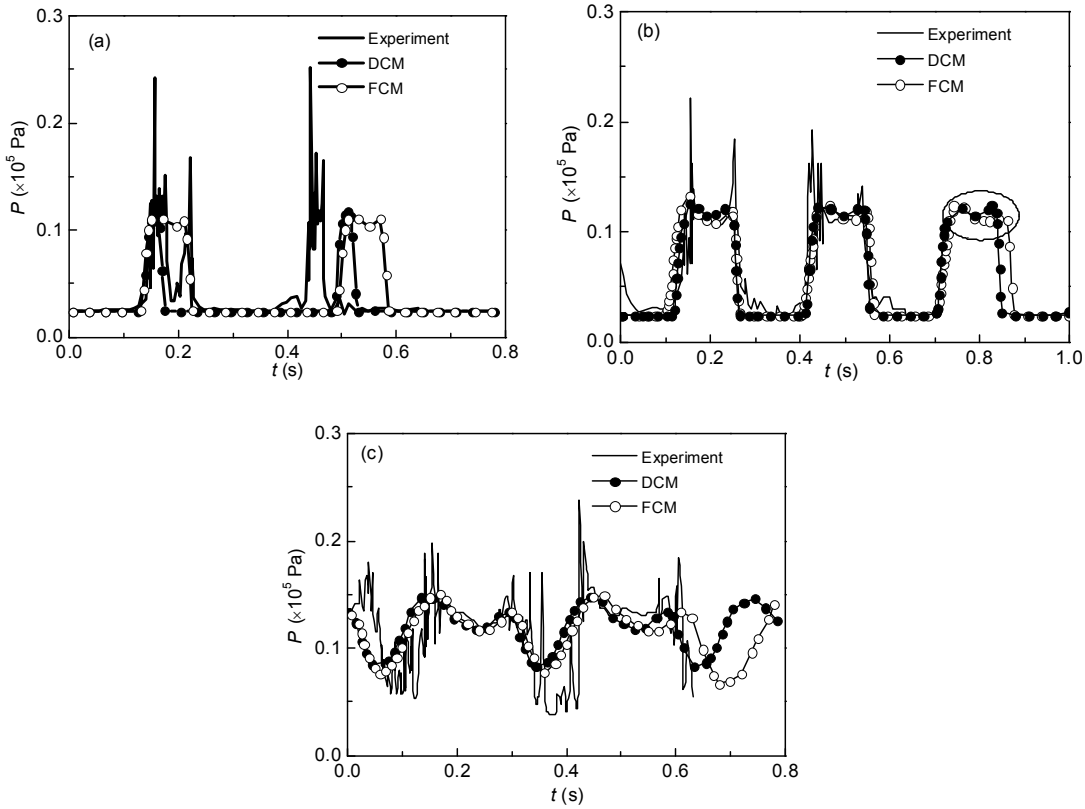

Figure 14 Instantaneous pressure fluctuations at different positions at σ=1.25. (a) x/c=0.3; (b) x/c=0.5; (c) x/c=0.7.

Table 1 Periodical characteristics of unsteady cavitation at x/c=0.5 with σ=1.25.

	Experiment	FCM	Relative error of FCM (%)	DCM	Relative error of DCM (%)
Period (s)	0.276	0.297	7.79	0.292	5.80
f (Hz)	3.625	3.36	–7.31	3.425	–5.52
$St=fc/U$	0.102	0.095	–6.86	0.0964	–5.49

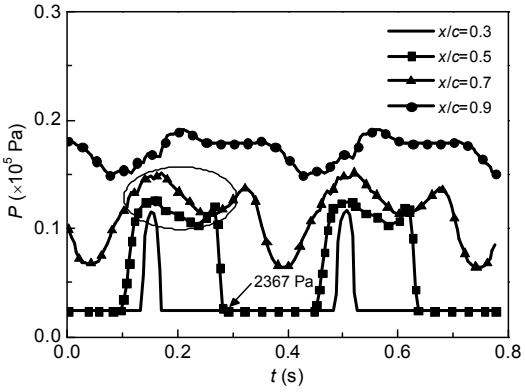

Figure 15 Instantaneous pressure fluctuations at different positions with DCM at σ=1.25.

and shedding before x/c=0.7. In addition, the fluctuation intensity decreases because of the decreases of the bubble numbers. The trend is more obvious compared to the curve for x/c=0.9.

5 Conclusions

The quasi-steady and unsteady cavitating flows through a NACA66 hydrofoil were modeled with the CFD approaches. The mathematical framework was based on the mixture homogenous model and the additional vapor mass fraction transfer equation. Two cavitation models: FCM and DCM, were used to calculate the cavitating flow. Comparisons with the experimental observations were performed to evaluate the feasibility of DCM for the modeling of the unsteady cloud cavitation. The following conclusions are drawn.

For cavitation number is equal to 1.34, the cavitating flow can be considered to be quasi-steady, and the pressure fluctuation is small enough to be neglected. No shedding of the cavity is observed. The computed discharge coefficient C_p and cavity length of both DCM and FCM agree well with the experiments. The cavity length decreases as Reynolds number increases.

For cavitation number is smaller than 1.25, the cavitating flow becomes highly unstable that the pressure fluctuation increases sharply in contrast to the case of σ=1.34. The periodical variation of C_p, and the frequency of the developing of the cavity are correctively modeled by DCM.

The results of DCM show its ability to simulate the transient characteristics for the highly unsteady cloud cavitation flow.

This work was supported by the National Natural Science Foundation of China (Grant No. 51276157) and Zhejiang Provincial Natural Science Foundation (Grant No. LY12E060026).

1 Coutier D O, Reboud J L, Delannoy Y. Numerical simulation of the unsteady behaviour of cavitating flows. Int J Numer Meth Fl, 2003, 42: 527–548
2 Coutier D O, Fortes P R, Reboud J L. Simulation of unsteady cavitation with a two-equation turbulence model including compressibility effects. J Turbul, 2002, 3: 058–075
3 Lu C J, He Y S, Chen X, et al. Numerical and experimental research on cavitating flows. New Trends in Fluid Mechanics Research. In: Proceedings of the 5th International Conference on Fluid Mechanics, 2007. 45–52
4 Senocak I, Shyy W. Interfacial dynamics-based modelling of turbulent cavitating flows, Part-1: Model development and steady-state computations. Int J Numer meth Fl, 2004, 44: 975–995
5 Singhal A K, Athavale M M, Li H Y. Mathematical basis and validation of the full cavitation model. J Fluids Eng Trans ASME, 2002, 124: 617–624
6 Senocak I, Shyy W. Evaluation of cavitation models for Navier-Stoke computation. Proc FEDSM, 2002, 2: 31011
7 Huang B, Wang G Y, Yu Z Y, et al. Detached-eddy simulation for time-dependent turbulent cavitating flows. Chin J Mech Eng-en, 2012, 25: 484–490
8 Merkle C L, Feng J, Buelow P E O. Computational modeling of the dynamics of sheet cavitation. In: Proceedings of the 3rd International Symposium on Cavitation, Grenoble, 1998
9 Kunz R F, Boger D A, Stinebring D R, et al. A preconditioned Navier-Stokes method for two-phase flows with application to cavitation prediction. Comput Fluids, 2000, 29: 849–875
10 Senocak I, Shyy W. Interfacial dynamics-based modelling of turbulent cavitating flows, Part-2: Time-dependent computations. Int J Numer meth Fl, 2004, 44: 997–1016
11 Sauer J, Schnerr G H. Unsteady cavitating flow: a new cavitation model based on a modified front capturing method and bubble dynamics. In: Proceedings of ASME Fluid Engineering Summer Conference, Boston, 2000
12 Zhang X B, Qiu L M, Gao Y, et al. Computational fluid dynamic study on cavitation in liquid nitrogen. Cryogenics, 2008, 48: 432–438
13 Cao X L, Zhang X B, Qiu L M, et al. Validation of full cavitation model in cryogenic fluids. Chin Sci Bull, 2009, 54: 1633–1640
14 Lohrberg H, Stoffel B, Fortes P R, et al. Numerical and experimental investigations on the cavitating flow in a cascade of hydrofoils. Exp Fluids, 2002, 33: 578–586
15 Park S, Rhee S H. Numerical analysis of the three-dimensional cloud cavitating flow around a twisted hydrofoil. Fluid Dyn Res, 2013, 45: 1–10
16 Ji B, Luo X, Wu Y, et al. Numerical analysis of unsteady cavitating turbulent flow and shedding horse-shoe vortex structure around a twisted hydrofoil. Int J Multiphase Flow, 2013, 51: 33–43
17 Zhang X B, WU Z, Xiang S J, et al. Modeling cavitation flow of cryogenic fluids with thermodynamic phase-change theory. Chin Sci Bull, 2013, 58: 567–574
18 Hosangadi A, Ahuja V. Numerical study of cavitation in cryogenic fluids. J Fluid Eng Trans ASME, 2005, 127: 267–281
19 Wu J Y, Wang G Y, Shyy W. Time-dependent turbulent cavitating flow computations with interfacial transport and filter-based models. Int J Numer Meth Fl, 2005, 49: 739–761
20 Tseng, C C. Turbulence and cavitation models for time-dependent turbulent cavitating flow. Acta Mech Sinica, 2011, 4: 473–487
21 Leroux J B, Astolfi J A, Billard J Y. An experimental study of unsteady partial cavitation. J Fluids Eng Trans ASME, 2004, 126: 94–101
22 Ji B, Luo X W, Peng X X, et al. Three-dimensional large eddy simulation and vorticity analysis of unsteady cavitating flow around a twisted hydrofoil. J Hydrod, 2013, 25: 510–519
23 Huang B, Yin L Y, Wang G Y, et al. Combined experimental and computational investigation of unsteady structure of sheet/cloud cavitation. J Fluids Eng Trans ASME, 2013, 135: 0713017
24 Leroux J B, Coutier D O, Astolfi J A. A joint experimental and numerical study of mechanisms associated to instability of partial cavitation on two-dimensional hydrofoil. Phys Fluids, 2005, 17, 052101: 1–8
25 Callenaere M, Franc J P, Michel J. The cavitation instability induced by the development of a re-entrant jet. J Fluid Mech, 2001, 444: 223–256
26 Kubota A, Kato H, Yamaguchiy H. A new modelling of cavitating flows: a numerical study of unsteady cavitation on a hydrofoil section. J Fluid Mech, 1992, 240: 59–96
27 Ji B, Luo X W, Wu Y L. Unsteady cavitating flow around a hydrofoil simulated using the partially-averaged Navier-Stokes model. Chin Phys Lett, 2012, 076401: 1–5
28 Huang B, Wang G Y. Experimental and numerical investigation of unsteady cavitating flows through a 2D hydrofoil. Sci China Tech Sci, 2011, 54: 1801–1812